Academic Science Journal

# Synthesis, Characterization and Dielectric Properties of Nickel and Copper Ferrite Embedded in Poly (Vinyl Alcohol) Films

**Omar G. Hammoodi**

Department of Chemistry, College of Science, University of Diyala

omarghazih@gmail.com

**Received: 4 January 2024** **Accepted: 5 March 2024**

**Published: 28 April 2025**

**DOI:** https://dx.doi.org/10.24237/ASJ.03.02.844A

## Abstract

In this research, the $NiFe_2O_4$ and $CuFe_2O_4$ nanoparticles were synthesized by sol-gel auto combustion technique, and diagnosed with various techniques such as infrared (FTIR), X-ray diffraction (XRD) and Field Emission Scaning Elecron Microscopy (FESEM). Diagnostic results showed obtaining (Ni and Cu) nanoparticles. Then (PVA, $NiFe_2O_4$/PVA and $CuFe_2O_4$/PVA) films were prepared, and their electrical conductivity studied using LCR device, and they were (0.00000000892848, 0.0000149 and 0.00000699889) for (PVA, $NiFe_2O_4$/PVA and $CuFe_2O_4$/PVA), respectively. Nickel and copper ferrite nanoparticles showed apparent increase in electrical conductivity for the pure polymer.

**Keywords:** Ferrites embedded PVA, Nickel ferrite, Copper ferrite, Dielectric properties.

## Introduction

Ferrite exhibits a crystalline structure in three dimensions, described by the chemical formula $MO.Fe_2O_3$, it comprises two iron atoms and three oxygen atoms. The term MO encompasses various metal oxides, with manganese, zinc, nickel, and others being potential components, the incorporation of different metal oxides holds the potential to modify the properties of ferrite, rendering it adaptable for diverse applications [1]. The utilization of metal ferrite materials spans across a spectrum of applications and technologies, driven by their notable electrical and magnetic properties [2-5]. Spinel ferrites [6] have been a subject of extensive investigation over an extended period, primarily attributed to their efficacy in high-frequency devices. In recent developments, ferrite materials have seen diversification in morphologies, including films [7], flakes [8], and hollow nanospheres [9], and macroporous particles [10]. These varied structures were successfully synthesized and applied as anode materials, contributing to magnify properties in Lithium-ion Batteries (LIBs), supercapacitor, ion batteries cell …etc., despite these studies, this method needs for further enhancement in discharge capacity and rate performances, particularly at high charge-discharge rates, to fully realize their practical potential across various applications [11,12]. To address this problem, a diverse array of preparation methods were explored. These methods encompass chemical precipitation, hydrothermal processing, micro-emulsion routes, sol-gel processing, aerosol-vapor methods, sonochemistry, and high-temperature decomposition of organic precursors [13-16]. Notably, the sol-gel auto-combustion process has recently emerged as a proposed technique for ferrite synthesis, contributing to the repertoire of preparation methods [17-20]. The aim of the current study is to synthesize nickel ferrite and copper ferrite nanoparticles, then characterize oxides by using different techniques (FTIR, XRD, FESEM), then polymeric films are prepared from these oxides and PVA as a matrix, and then the electrical properties of the prepared films are measured.

## Experimental part:

### Chemicals:

Chemical used in experiments were $Ni(NO_3)_2.6H_2O$, $Cu(NO_3)_2.6H_2O$, $Fe(NO_3)_2.9H2O$, $NH_4OH$, citric acid and poly vinyl alcohol. The purity of the chemicals and solvents used was between 98-99% and they were used without purification or recrystallization.

### Procedure:

### Preparation of nickel ferrite ($NiFe_2O_4$):

For the synthesis of $NiFe_2O_4$ nanoparticle compound, the sol-gel technique was employed. This involved utilizing molar ratios of (1:2:3) for $Ni(NO_3)_2.6H_2O$, $Fe(NO_3)_3$ $.9H_2O$, and citric acid. The nitrates salts and citric acid were individually dissolved in distilled water and subsequently combined in a large flask. The ingredients were thoroughly mixed by magnetic stirrer and the pH of solution was adjusted to be 7. The contents were homogenized at room temperature for 35 minutes and then the temperature rises to 95°C. The gases started to rise, and the gel was formed. After 30 min., the gel started to flare forming a Xerogel, which is grinded with mortar. The xerogel was then placed in furnace for calcined at a temperature of 600°C for two hours at heating rate of (10 deg / min) to obtain the required $NiFe_2O_4$ nanoparticles.

**Preparation of copper ferrite ($CuFe_2O_4$):**

For the production of $CuFe_2O_4$ nanoparticle compound, the sol-gel methodology was applied. This method employed molar ratios of (1:2:3) for $Cu(NO_3)_2.6H_2O$, $Fe(NO_3)_3.9H_2O$, and citric acid. The nitrates salts and citric acid were separately dissolved in distilled water and subsequently amalgamated in a sizable flask. The ingredients underwent thorough mixing facilitated by a magnetic stirrer, and the pH of the solution was adjusted to 7. The amalgamated contents were homogenized at room temperature for 35 minutes, followed by a temperature increase to 95°C. The release of gases ensued, leading to gel formation. Approximately half an hour later, the gel transitioned into a Xerogel, which was then ground using a mortar. Subsequently, it was subjected to calcination in a furnace at a temperature of 600°C for two hours, with a heating rate of (10 deg/min), yielding the desired $CuFe_2O_4$ nanoparticles.

**Preparation of the PVA, $NiFe_2O_4$/PVA and $CuFe_2O_4$/PVA:**

30 g of PVA (14000) were dissolved in 300 ml distilled water with continuous stirring at 70 °C, then the solution was left for overnight. 25 ml of PVA solution was poured in glass mold to prepare the pure PVA film. Moreover, 25 ml of stock solution (PVA solution) was placed in a 100 ml beaker and 0.2 g of (Ni,Cu) ferrites were added separately, with continuous vigorous stirring for 30 min, and left for 10 min., then sonicated for 10 min.. The final step is to pour the prepared solution into the glass mold and left for overnight to obtain the doped PVA films.

## Results and Discussion

**FTIR of Nickle Ferrite Nanoparticles:**

In the FTIR spectrum presented in Figure 1 for $NiFe_2O_4$, the absorption peak observed at 573.09 $cm^{-1}$ is likely associated with the (Fe-O) group within $NiFe_2O_4$. Conversely, the presence of a band at 444.2 $cm^{-1}$ is attributed to the octahedral metal (Ni-O). The disparity in absorption positions between tetrahedral and octahedral complexes within the $NiFe_2O_4$ crystal arises from the distinct distances between $Fe^{+3}$-$O^{-2}$ in the tetrahedral and octahedral sites. These distinctive features of spinal ferrite, along with the specific positions of these infrared bands, align with the expected ranges corresponding to $NiFe_2O_4$ [21].

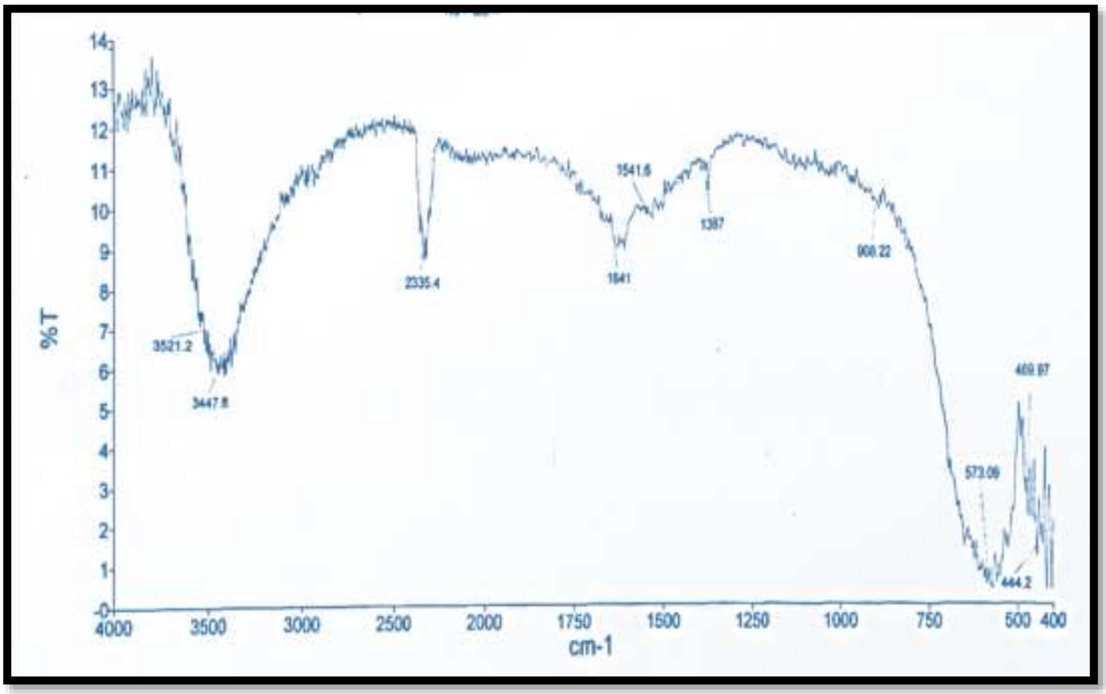

**Figure 1:** FTIR spectrum of $NiFe_2O_4$ nanoparticles.

### FTIR of $CuFe_2O_4$ nanoparticles:

The FTIR spectrum depicted in Figure 2 for $CuFe_2O_4$ nanoparticles reveals two distinct absorption bands. At 408.23 cm-1, the observed band is attributed to the vibration of the (Fe-O) bond, while the band at 556.94 $cm^{-1}$ agrees to the vibration of the (Cu-O) bond within the lattices of the ferrite spinel. These assignments are consistent with the positioning of these bonds in both octahedral and tetrahedral sites. The variation in frequency between these bands is a result of the differing lengths of the oxygen-metal bonds in octahedral and tetrahedral sites. Consequently, the stretching vibration exhibits a higher frequency at the tetrahedral site, whereas the vibration at the octahedral site is characterized by a lower frequency [22,23].

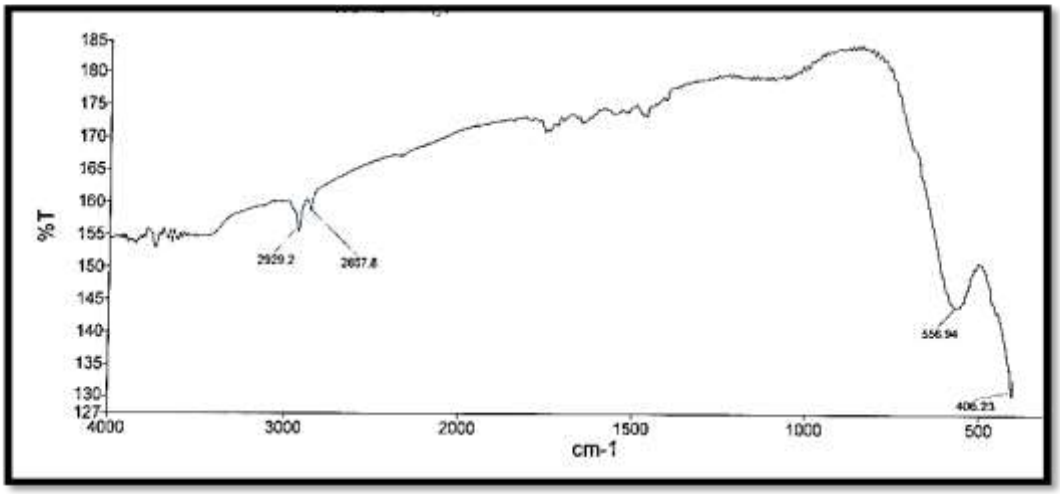

**Figure 2:** FTIR spectrum of $CuFe_2O_4$ nanoparticles.

**XRD of Nickle ferrite nanoparticles:**

Figure (**3**) displys the X-ray of nickle ferrite. All of the $NiFe_2O_4$ peaks are present: 30.29 (220), 35.7 (311), 37.31 (222), 43.36 (400), 53.80 (422), 57.36 (511), 62.92 (440), and 74.64 (533) [24]. Diffraction displys sharp lines. This indicates that the sample has a high degree of crystallinity. These planes correspond to the structure of $NiFe_2O_4$ nanoparticles. From the XRD data, the grain size of the prepared $NiFe_2O_4$ particles were calculated to be 33.18 nm, applying Debye-shearer equation.

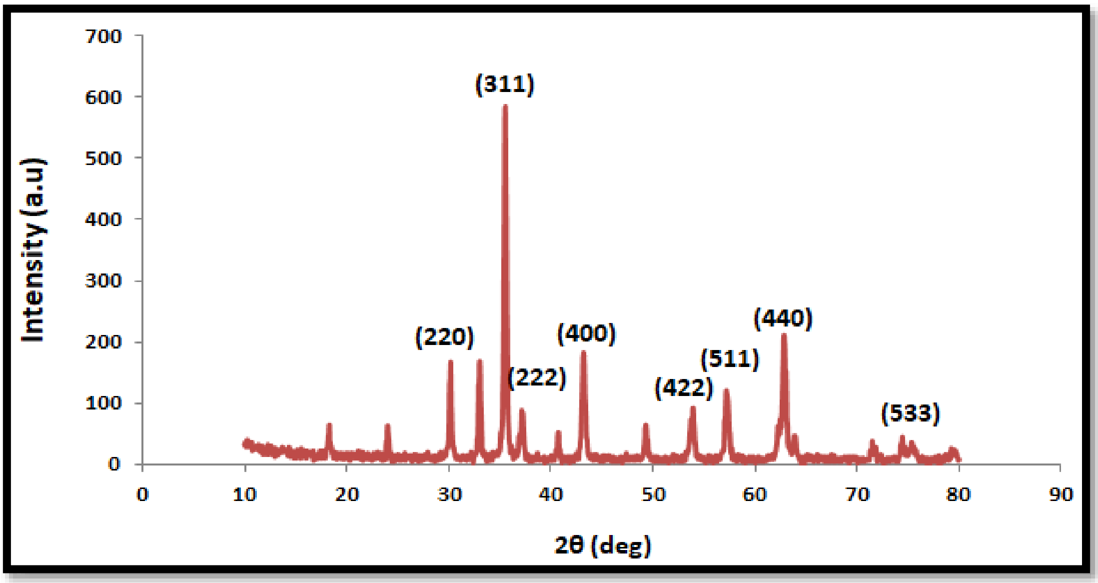

**Figure 3:** XRD of $NiFe_2O_4$ nanoparticles.

### XRD of Copper ferrite nanoparticles:

The XRD pattern presented in Figure 4 illustrates the diffraction pattern of $CuFe_2O_4$ nanoparticles, aligning closely with JCPDS card no. 00-034-0425. The XRD peaks exhibit broadened reflections associated with (101), (200), (103), (211), (400), (004), (422), (511), (224), and (440) planes. Additionally, there are discernible peaks indicating the presence of extra phases, such as CuO. The identified planes collectively correspond to the cubic spinel structure of $CuFe_2O_4$. The grain size of prepared $CuFe_2O_4$ particles were calculated to be 32.09 nm, applying Debye-shearer equation.

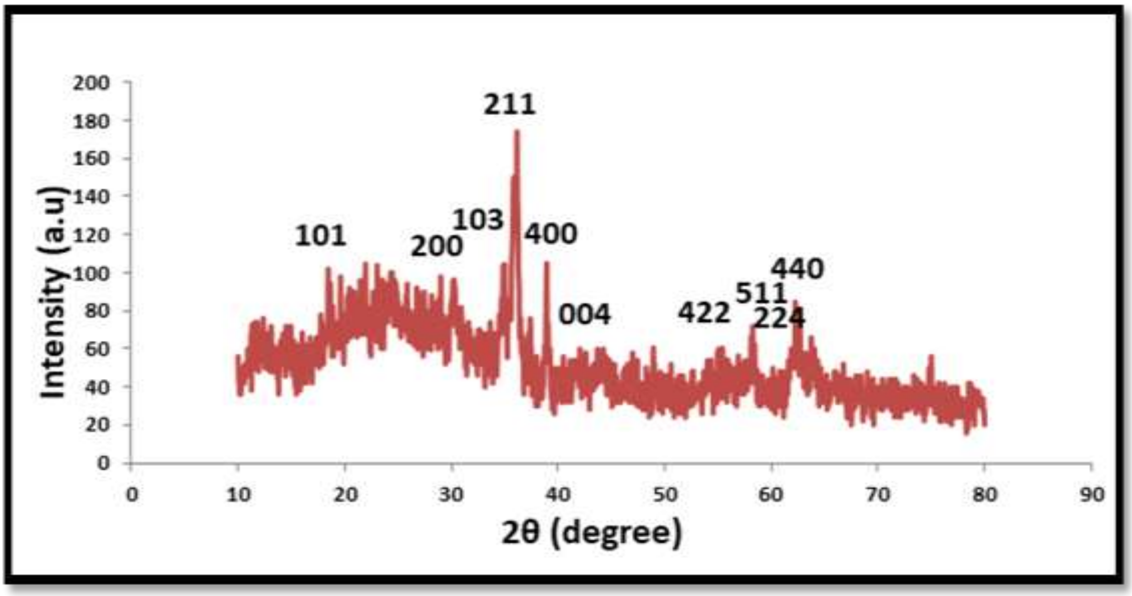

**Figure 4:** XRD of $CuFe_2O_4$ nanoparticles.

### FESEM of $NiFe_2O_4$ and $CuFe_2O_4$ nanoparticles

The structural morphology of the nanoparticles were tested using Field Emission Scanning Electron Microscopy (FESEM). Figure 5, displays the FESEM images of $NiFe_2O_4$ and $CuFe_2O_4$ nanoparticles. The nanoparticles structural of $NiFe_2O_4$ compound is cubic with grain sizes range 36.74 nm and for $CuFe_2O_4$ is tetragonal with grain sizes range 54.18nm.

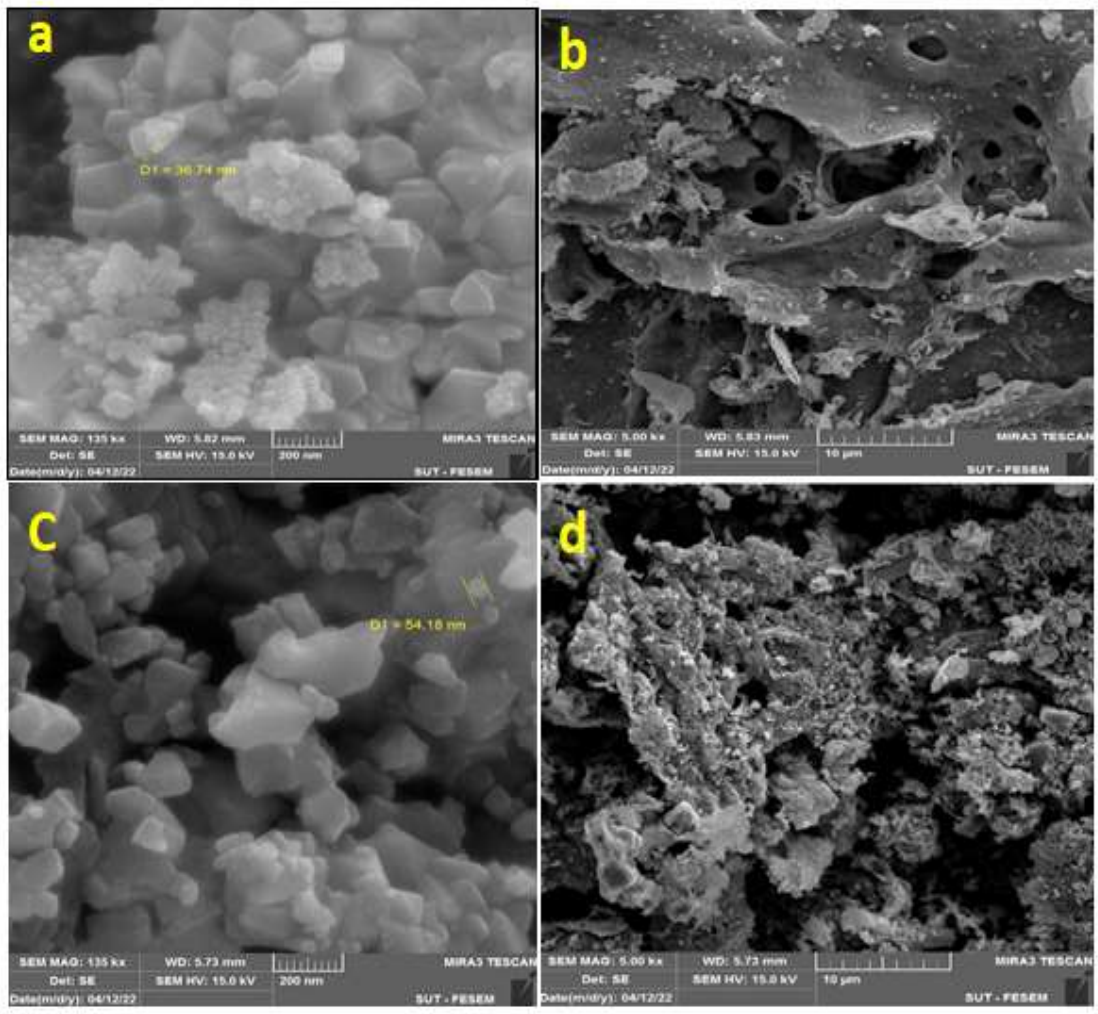

**Figure 5:** (a,b) FESEM images of $NiFe_2O_4$ and (c,d) $CuFe_2O_4$ nanoparticles.

**The dielectric properties:**

To evaluate the dielectric characterization of fabricated films, circular samples with a diameter of 3 cm were precision-cut to match the electrode diameter of the (GWINSTEK LCR-8105G) LCR meter. The dielectric properties, including real permittivity ($\varepsilon'$), imaginary permittivity ($\varepsilon''$), loss factor ($\tan\delta$), and current conductivity ($\sigma_{Ac}$), were derived from the measured data. Dielectric investigation were conducted over a range of frequencies spanning from 60 kHz to 1000 kHz at a temperature of 25 $^{o}$C. The determination of dielectric factors involved the utilization of the complex permittivity ($\varepsilon^*$) in the respective equation [25-27]:

$$\mathcal{E}* = \mathcal{E}'(\omega) - \mathcal{E}''(\omega) \qquad (1)$$

In the provided equation, ($\varepsilon'$) denotes the real permittivity, and ($\varepsilon''$) represents the imaginary permittivity. The angular frequency ($\omega$) is expressed as ($\omega = 2\pi f$), where (f) signifies the applied frequency. The dielectric permittivity ($\varepsilon'$) was determined using capacitance (C) through the following formula:

$$\varepsilon' = \frac{C\,d}{\varepsilon_\circ A} \qquad (2)$$

In this specified context, the symbol (d) signifies the film's thickness, (A) denotes the area of the electrodes, ($\varepsilon_0$) stands for the free space permittivity, equal to $8.85 \times 10^{-12}$ F·m$^{-1}$, and (tan δ) represents the tangent delta.

$$\varepsilon''(\omega) = \varepsilon'(\omega) \, . \tan\delta\,(\omega) \qquad (3)$$

The alternating current conductivity ($\sigma$ ac) can be calculated using the following equation:

$$\sigma = \varepsilon_o \varepsilon' \omega \tan\delta \quad (4)$$

The dielectric properties investigation involved examining pure PVA and its doped films with $NiFe_2O_4$ and $CuFe_2O_4$ nanocomposites across a frequency range of 60 kHz to 1000 kHz, and the results are depicted in Figures 6-8. The profiles illustrate the variations in real permittivity ($\varepsilon'$), imaginary permittivity ($\varepsilon''$), and conductivity ($\sigma$ ac) for the the loaded $NiFe_2O_4$/PVA and $CuFe_2O_4$/PVA nanocomposite and pure PVA films. Figures 6 and 7 indicate a gradual reduction in both ($\varepsilon'$) and ($\varepsilon''$) values as the frequency increases, as observed from the logarithmic plot. At lower frequencies, higher values of ($\varepsilon'$) and ($\varepsilon''$) are reached, diminishing rapidly with the ascending frequency. This phenomenon is explained by the gradual rotation of the field in the low-frequency domain, providing ample time for the alignment of permanent and induced dipoles with the applied field, consequently amplifying polarization. The heightened ($\varepsilon'$) values, especially at lower frequencies, are ascribed to interfacial polarization [27-30]. Moreover, in the composite films incorporating the nano fillers ($NiFe_2O_4$ and $CuFe_2O_4$), the imaginary permittivity primarily results from current leakage. The introduction of a higher content of conductive fillers ($NiFe_2O_4$ and $CuFe_2O_4$) is likely to create additional conductive paths, leading to increased current leakage. Consequently, an observable rise in the value of ($\varepsilon''$) is noted with the incorporation of conductive fillers into the PVA films [31].

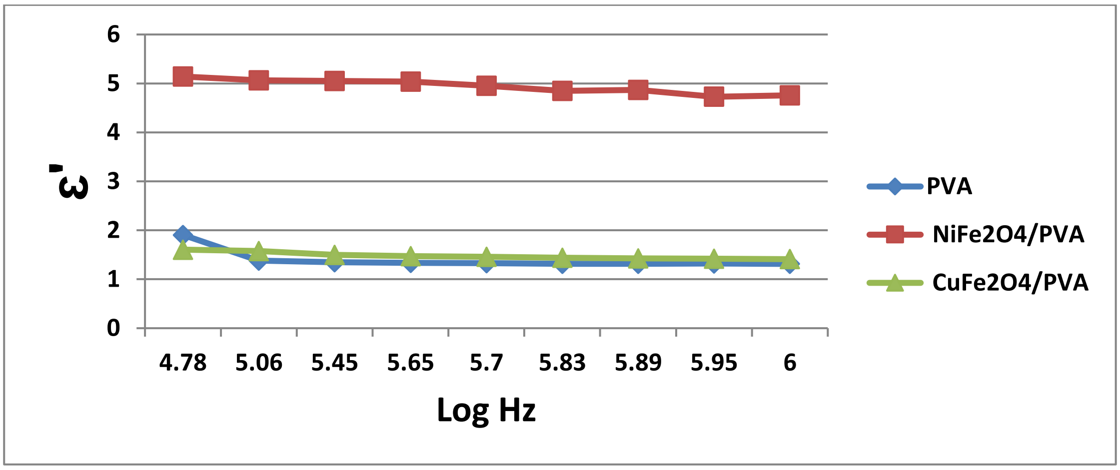

**Figure 6:** Relation between the real permittivity ε' and the frequency change values of PVA, $NiFe_2O_4$/PVA and $CuFe_2O_4$/PVA.

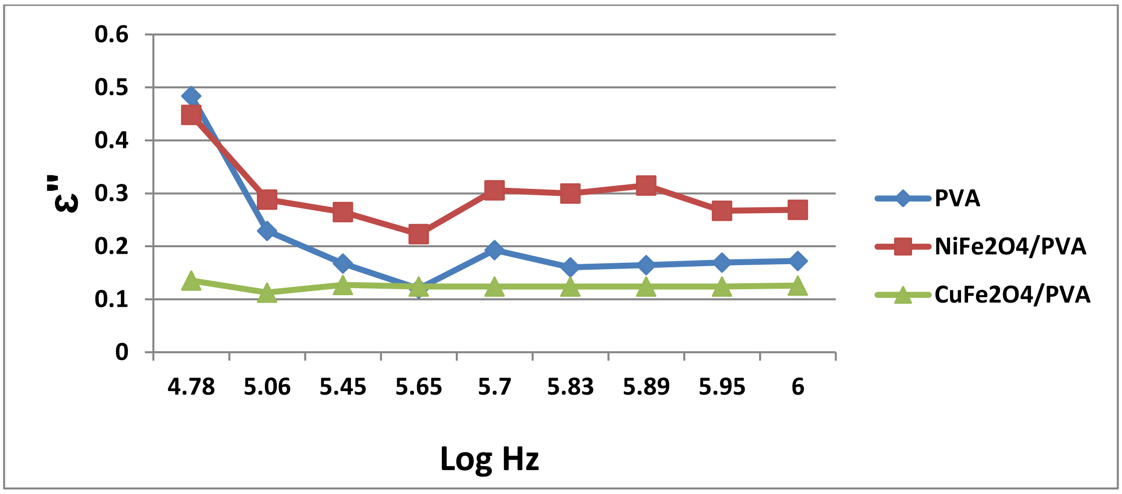

**Figure 7:** Relation between imaginary permittivity ε" and frequency change values of PVA, $NiFe_2O_4$/PVA and $CuFe_2O_4$/PVA.

On the flip side, the AC electrical conductivity (σ ac) observed in all fabricated nanocomposite films initiates at a low level and steadily rises with increasing frequency, as depicted in Figure 8. The logarithmic conduction diagram plotted against frequency indicates that, initially, both the pure PVA film and the films incorporating nano-fillers ($NiFe_2O_4$ and $CuFe_2O_4$) exhibit insulating behavior at lower frequencies. However, as the frequency escalates from 60,000 Hz to 1000 kHz, their behavior transitions from insulator to semiconductor, except for the polyvinyl alcohol film, which remains insulating. This behavior is contingent on the electrical conductivity value. The incorporation of nanomaterials impacts the electrical conductivity (σ ac) within the nanocomposite films. The introduction of nanomaterials to polymeric films results in a proportional increase in the electrical conductivity of these films. This rise is linked to the heightened concentration of charge carriers, originating from the presence of free electrons in the nano-oxides [27,31,32].

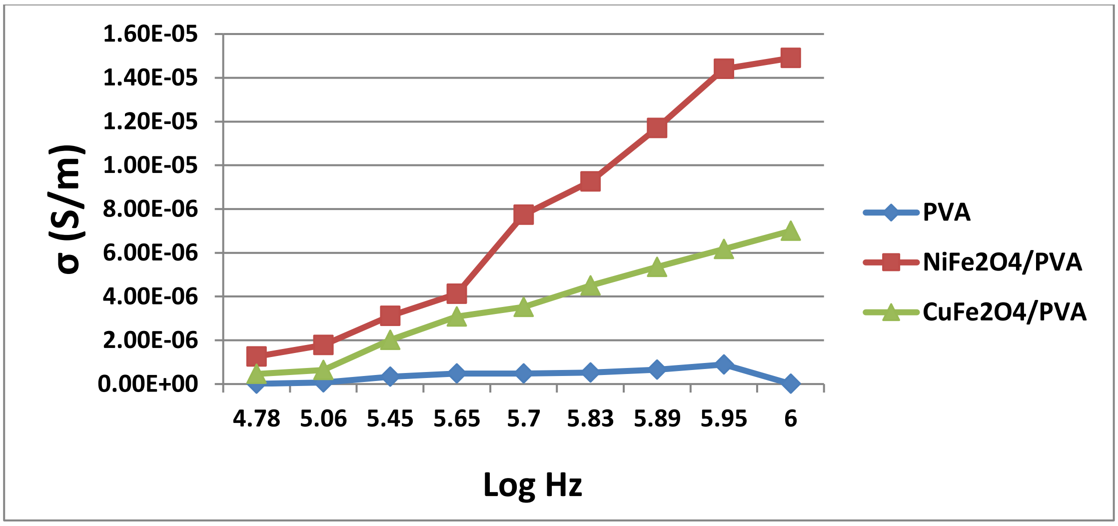

**Figure 8:** Relation of conductivity with frequency values of PVA, $NiFe_2O_4$/PVA and $CuFe_2O_4$/PVA.

## Conclusion

$NiFe_2O_4$ and $CuFe_2O_4$ nanoparticles were prepared using sol-gel processes. FTIR test confirmed to obtain Nickle and copper ferrites. XRD revealed single phase spinal structure. FESEM images showed prepared nanoparticles in nano range. Experimental results exhibit that the electrical conductivity of prepared composites increased with increase the frequencies and $NiFe_2O_4$/PVA conductivity (0.00000699889) more than $CuFe_2O_4$/PVA (0.0000149) and two composites more than PVA conductivity (0.00000000892848) that indicates the apparent effect of the Nickle ferrite copper ferrite on the electrical properties of poly vinyl alcohol polymer.

**Source of funding:** None

**Conflict of interest:** The author declare that is no conflict of interest

## References

[1] A. T. Apostolov, I. N. Apostolova, J. M. Wesselinowa, MO. $Fe_2O_3$ nanoparticles for self-controlled magnetic hyperthermia, Journal of Applied Physics, 109(8), (2011), DOI(https://doi.org/10.1063/1.3580476)

[2] A. H. Majeed, M. M. Khan, J. R. Jennings, Ferrites and ferrite-based K. O.composites for energy conversion and storage applications, Critical Reviews in Solid State and Materials Sciences,1-49(2023), DOI(https://doi.org/10.1080/10408436.2023.2272963)

[3] T. Fatmawati, M. Shiddiq, B. Armynah, D. Tahir, Synthesis Methods of $Fe_3O_4$ Nanoparticles for Biomedical Applications, Chemical Engineering & Technology, 46(11), 2356-2366(2023), DOI(https://doi.org/10.1002/ceat.202200384)

[4] L. E. Caldeira, C. S. Erhardt, F. R. Mariosi, J. Venturini, R. Y. S. Zampiva, O. R. K. Montedo, S. R. Braganca, Correlation of synthesis parameters to the structural and magnetic properties of spinel cobalt ferrites ($CoFe_2O_4$)–an experimental and statistical study, Journal of Magnetism and Magnetic Materials, 550, 169128(2022), DOI(https://doi.org/10.1016/j.jmmm.2022.169128)

[5] M. Mojahed, H. R. Dizaji, A. Gholizadeh, Structural, magnetic, and dielectric properties of Ni/Zn co-substituted $CuFe_2O_4$ nanoparticles, Physica B: Condensed Matter, 646, 414337(2022), DOI(https://doi.org/10.1016/j.physb.2022.414337)

[6] H. Qin, Y. He, P. Xu, D. Huang, Z. Wang, H. Wang, C. Wang, Spinel ferrites ($MFe_2O_4$): Synthesis, improvement and catalytic application in environment and energy field, Advances in Colloid and Interface Science, 294, 102486(2021), DOI(https://doi.org/10.1016/j.cis.2021.102486)

[7] Y. Q. Chu, Z. W. Fu, Q. Z. Qin, Cobalt ferrite thin films as anode material for lithium ion batteries, Electrochimica Acta, 49(27), 4915-4921(2004), DOI(https://doi.org/10.1016/j.electacta.2004.06.012)

[8] P. Lavela, J. L. Tirado, $CoFe_2O_4$ and $NiFe_2O_4$ synthesized by sol–gel procedures for their use as anode materials for Li ion batteries, Journal of power sources, 172(1), 379-387(2007), DOI(https://doi.org/10.1016/j.jpowsour.2007.07.055)

[9] Y. Wang, D. Su, A. Ung, J. H. Ahn, G. Wang, Hollow CoFe2O4 nanospheres as a high capacity anode material for lithium ion batteries, Nanotechnology, 23(5), 055402(2012), DOI(10.1088/0957-4484/23/5/055402)

[10] Z. H. Li, T. P. Zhao, X. Y. Zhan, D. S. Gao, Q. Z. Xiao, G. T. Lei, High capacity three-dimensional ordered macroporous $CoFe_2O_4$ as anode material for lithium ion batteries, Electrochimica Acta, 55(15), 4594-4598(2010), DOI(https://doi.org/10.1016/j.electacta.2010.03.015)

[11] H. Xia, D. Zhu, Y. Fu, X. Wang, $CoFe_2O_4$-graphene nanocomposite as a high-capacity anode material for lithium-ion batteries, Electrochimica Acta, 83, 166-174(2012), DOI(https://doi.org/10.1016/j.electacta.2012.08.027)

[12] S. Liu, J. Xie, C. Fang, G. Cao, T. Zhu, X. Zhao, Self-assembly of a $CoFe_2O_4$/graphene sandwich by a controllable and general route: towards a high-performance anode for Li-ion batteries, Journal of Materials Chemistry, 22(37), 19738-19743(2012), DOI(https://doi.org/10.1039/C2JM34019D)

[13] B. Bekele, A. Degefa, F. Tesgera, L. T. Jule, R. Shanmugam, L. Priyanka Dwarampudi, K. Ramasamy, Green versus chemical precipitation methods of preparing zinc oxide nanoparticles and investigation of antimicrobial properties, Journal of Nanomaterials, 2021, 1-10(2021), DOI(https://doi.org/10.1155/2021/9210817)

[14] L. Wang, M. Zhang, Study on synthesis and magnetic properties of Nd2Fe14B nanoparticles prepared by hydrothermal method, Journal of Magnetism and Magnetic Materials, 507, 166841(2020), DOI(https://doi.org/10.1016/j.jmmm.2020.166841)

[15] A. Das, K. Natarajan, S. Tiwari, A. K. Ganguli, Nanostructures synthesized by the reverse microemulsion method and their magnetic properties, Materials Research Express, 7(10), 104001(2020), DOI(10.1088/2053-1591/abbb55)

[16] A. K. Vivekanandan, V. Subash, S. M. Chen, S. H. Chen, Sonochemical synthesis of nickel-manganous oxide nanocrumbs decorated partially reduced graphene oxide for efficient electrochemical reduction of metronidazole, Ultrasonics Sonochemistry, 68, 105176(2020), DOI(https://doi.org/10.1016/j.ultsonch.2020.105176)

[17] L. Li, F. Jing, J. Yan, J. Jing, W. Chu, Highly effective self-propagating synthesis of $CeO_2$-doped $MnO_2$ catalysts for toluene catalytic combustion, Catalysis Today, 297, 167-172(2017), DOI(https://doi.org/10.1016/j.cattod.2017.04.053)

[18] H. Bahiraei, C. K. Ong, The role of iron ions on microstructural and magnetic properties of MgCuZn ferrites prepared by sol-gel auto-combustion process, Materials Research Bulletin, 111, 195-201(2019), DOI(https://doi.org/10.1016/j.materresbull.2018.11.026)

[19] M. Harun-Or-Rashid, M. M. Rahman, M. Arifuzzaman, A. A. Hossain, Structural, magnetic, and electrical properties of $Ni_{0.38-x}Cu_{0.15+y}Zn_{0.47+x-y}Fe_2O_4$ synthesized by sol–gel auto-combustion technique, Journal of Materials Science: Materials in Electronics, 32, 13761-13776(2021), DOI(https://doi.org/10.1007/s10854-021-05953-z)

[20] D. Çoban Özkan, A. Türk, E. Celik, Synthesis and characterizations of sol–gel derived $LaFeO_3$ perovskite powders, Journal of Materials Science: Materials in Electronics, 31, 22789-22809(2020),DOI(https://doi.org/10.1007/s10854-020-04803-8)

[21] F. Majid, J. Rauf, S. Ata, I. Bibi, A. Malik, S. M. Ibrahim, M. Iqbal, Synthesis and characterization of $NiFe_2O_4$ ferrite: Sol–gel and hydrothermal synthesis routes effect on magnetic, structural and dielectric characteristics, Materials Chemistry and Physics, 258, 123888(2021),DOI(https://doi.org/10.1016/j.matchemphys.2020.123888)

[22] C. Dey, D. De, M. Nandi, M. M. Goswami, A high performance recyclable magnetic $CuFe_2O_4$ nanocatalyst for facile reduction of 4-nitrophenol, Materials Chemistry and Physics, 242, 122237(2020), DOI(https://doi.org/10.1016/j.matchemphys.2019.122237)

[23] S. Bhukal, M. Dhiman, S. Bansal, M. K. Tripathi, S. Singhal, Substituted Co–Cu–Zn nanoferrites: synthesis, fundamental and redox catalytic properties for the degradation of methyl orange, RSC Adv., 6, 1360–1375(2016), DOI(https://doi.org/10.1039/C5RA22561B)

[24] S. B. Gopale, G. N. Kakade, G. D. Kulkarni, V. Vinayak, S. P. Jadhav, K. M. Jadhav, X-ray diffraction, infrared and magnetic studies of $NiFe_2O_4$ nanoparticles, In Journal of Physics, In: Conference Series, 1644(1), 012010(2020), DOI(10.1088/1742-6596/1644/1/012010)

[25] I. Latif, E. E. AL-Abodi, D. H. Badri, J. Al Khafagi, Preparation, characterization and electrical study of (carboxymethylated polyvinyl alcohol/ZnO) nanocomposites, American Journal of Polymer Science, 2(6), 135-140(2012), DOI(10.5923/j.ajps.20120206.01)

[26] I. A. Latif, H.M. Abdullah, and M. H. Saleem, Electrical and swelling study of different prepared hydrogel, Am J Polym Sci, 6(2), 50-57(2016), DOI(10.5923/j.ajps.20160602.04)

[27] I. Latif, T. B. Alwan, and A.H. Al-Dujaili, Low frequency dielectric study of PAPA-PVA-GR nanocomposites, Nanoscience and Nanotechnology, 2(6), 190-200(2012), DOI(10.5923/j.nn.20120206.07)

[28] Y. C. Li, R. K. Y. Li, S. C. Tjong, Frequency and temperature dependences of dielectric dispersion and electrical properties of polyvinylidene fluoride/expanded graphite composites, Journal of Nanomaterials, 2010(1), 261748(2010), DOI(https://doi.org/10.1155/2010/261748)

[29] G. C. Psarras, Conductivity and dielectric characterization of polymer nanocomposites, Physical properties and applications of polymer nanocomposites, 31-69(2010), DOI(https://doi.org/10.1533/9780857090249.1.31)

[30] A. H. Al-Agha, and I. A. Latif, The Study of Functionalization Effect (poly aniline (PAni) and thiocarbohydrazide (TCH)) on Electrical Properties of Graphene Oxide Nanoparticles, Diyala Journal For Pure Science, 12(3-part 1), (2016)

[31] A. H. Majeed, E. T. B. Al-Tikrity, and D. H. Hussain, Dielectric properties of synthesized ternary hybrid nanocomposite embedded in poly (vinyl alcohol) matrix films, Polymers and Polymer Composites, 29(7), 1089-1100(2021), DOI(https://doi.org/10.1177/0967391120951406)

[32] E. T. B. Al-Tikrity, I. F. Waheed, and S. M. Ali, Study of electrical properties of a reduced graphene-oxadiazole-2-thiol (rGS) PVA polymer composite, Polymers and Polymer Composites, 27(1), 11-19(2019), DOI(https://doi.org/10.1177/0967391118809439)